JOURNAL OF GEOPHYSICAL RESEARCH, VOL. 101, NO. B3, PAGES 5489-5498, MARCH 10, 1996

Finite amplitude folding of a continuously viscosity-stratified lithosphere

M.T. Zuber[1, 2]
Department of Earth and Planetary Sciences, Johns Hopkins University, Baltimore, Maryland

E.M. Parmentier
Department of Geological Sciences, Brown University, Providence, Rhode Island

Abstract. We study the development of finite amplitude folding of the lithosphere through the application of finite element models characterized by both discontinuous (layer over half-space) and continuous (strength envelope) viscosity distributions. Both models include strongly strain rate-dependent rheologies that approximate slip on pervasive faults. Folding with layers of uniform, contrasting viscosities is driven solely by the magnitudes of discontinuities in viscosity at layer interfaces; however, folds may also develop in a medium with a continuously varying viscosity distribution. The net driving force for folding in a region of continuous viscosity variation is the same as the driving force across a discontinuity with the same net viscosity contrast. Continuous and discontinuous viscosity variations give essentially identical fold growth rates if the depth over which the viscosity varies is small compared to the wavelength of folding or the depth of the viscosity variation. In the uniform viscosity layer model, flexural bending of the layer results in a state of extension on topographic highs and compression in topographic lows. In contrast, the strength envelope model is characterized by significant penetrative shortening near the surface that results in a state of compression everywhere along the fold. This model predicts layer thickening beneath fold troughs, as observed in the intraplate deformation zone in the central Indian Ocean. Buoyancy forces retard the rate of fold amplification but are inadequate to prevent folding for a range of realistic lithospheric rheological structures.

Introduction

The characteristic wavelength of folding in a medium that is rheologically layered perpendicular to the direction of shortening has long been recognized to be a sensitive function of thicknesses and viscosities (or strengths) of the layers [*Biot*, 1957]. Folding models that relate the dominant wavelength of folding to layer thickness and viscosity contrasts have been extensively applied to determine the relative viscosities of discretely layered strata on the geological outcrop scale [e.g., *Johnson*, 1970; *Fletcher*, 1974, 1977]. More recently, the observed wavelengths of much larger scale folds (~101-102 km) have been used to infer the vertical rheological structure of the mechanical lithosphere. Lithospheric-scale folds have been identified on the continents [*Biot*, 1961], in ocean basins [*Weissel et al.*, 1980], and on planetary surfaces such as Venus [*Campbell et al.*, 1983]. Models that address the nature of lithospheric-scale folding include analytical solutions for flexure of thin elastic [*Turcotte and Schubert*, 1982; *Karner and Watts*, 1983; *Karner and Weissel*, 1990a,b], viscoelastic [*Lambeck*, 1983] or elastic-plastic [*McAdoo and Sandwell*, 1985] plates; linearized analytical and numerical solutions of the Navier-Stokes equations for viscous flow for media with a single rheologically strong layer [*Zuber*, 1987a; *Martinrod and Davy*, 1992]; and numerical small-amplitude solutions for media that contain multiple strong lithospheric layers [*Ricard and Froidevaux*, 1986; Zuber, 1987b; *Zuber and Aist*, 1991].

A number of notable simplifications characterize previous lithospheric-scale folding models. First, as illustrated schematically in Figure 1, most models assumed viscosity or strength distributions that are discontinuous with depth, unlike the distribution of strength in the lithosphere as supported by rock mechanics experiments [*Byerlee*, 1968; *Brace and Kohlstedt*, 1980; *Kirby and Kronenberg*, 1987]. For example, Figure 1a represents the structure assumed in most flexural folding models, a strong, uniform rigidity layer that overlies a weak or inviscid substrate. For the structure in Figure 1a the primary driving force for fold development arises from the contrast in Young's modulus (for elastic models), viscosity (for viscous models), or yield stress (for plastic models) between the strong surface layer and the much weaker substrate. Since the lithosphere probably does not contain discrete layers of contrasting uniform strength, this model overestimates the tendency for folding instabilities to grow.

An alternative approach (Figure 1b) is to consider deformation of a continuously stratified medium in which strength is uniform near the surface and decreases as a simple exponential function of depth to approximate the temperature dependence of ductile strength in the lithosphere. In this case the strength profile is everywhere continuous, and the tendency for fold growth is driven by the viscosity gradient. However, additional driving terms that arise from folding of initially horizontal surfaces of constant viscosity have not been included in previous analytical models of this structure [*Biot*, 1960; *Zuber*, 1987a], and the models therefore underestimate the tendency for folds to grow. Neither models

[1]Also at Laboratory for Terrestrial Physics, NASA/Goddard Space Flight Center, Greenbelt, Maryland.

[2]Now at Department of Earth, Atmospheric, and Planetary Sciences, Massachusetts Institute of Technology, Cambridge.

Paper number 95JB02514.
0148-0227/96/95JB02514$05.00

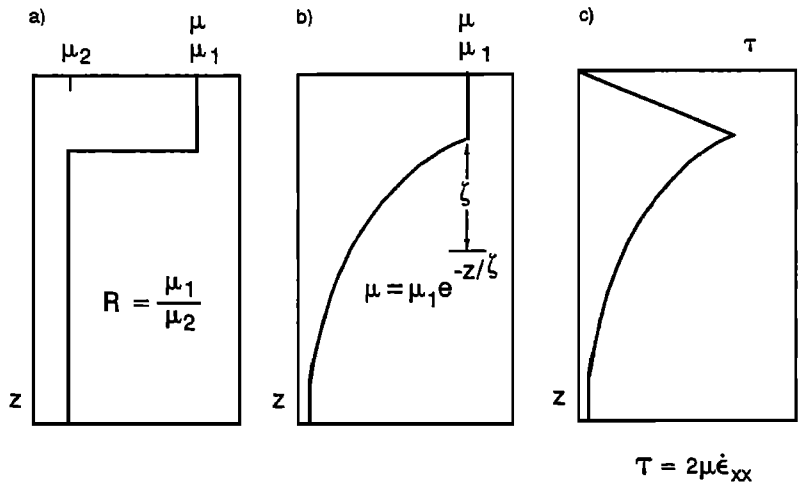

Figure 1. Schematic rheological representations of viscosity (μ) or strength ($\tau = 2\mu\dot{\varepsilon}_{xx}$) versus depth ($z$) for a model lithosphere in a state of horizontal compression. (a) Structure corresponds to a high strength layer that overlies a lower strength layer. (b) Structure is characterized by a high strength layer that overlies a layer with exponentially decreasing strength. (c) Structure corresponds to vertical strength profile in the lithosphere based on laboratory experiments of brittle (straight line) and ductile (curved line) deformation. In models in Figures 1b and 1c, strength is everywhere continuous within the lithosphere.

with discrete layers nor exponental viscosity variation closely approximate the distribution of strength of the lithosphere (Figure 1c) and both are valid only for infinitesimal fold amplitudes. Thus these formulations cannot be applied in areas that have undergone large strains that are characteristic of some fold belts [*cf. Platt et al.*, 1983].

In this study we develop a more realistic quantitative representation of lithospheric-scale folding, by constructing finite element models of a lithosphere undergoing uniform horizontal shortening. These models incorporate general viscosity structures, treat both Newtonian and non-Newtonian flow, and are valid at finite strains. To provide a physical foundation for our analysis, we first compare finite element solutions for Newtonian viscous folding at small strains with previously published linearized infinitesimal amplitude solutions for the same rheological structures. We then examine the effect on the style of folding of a non-Newtonian viscosity distribution that more realistically represents the rheology of the lithophere and address how well the simplified structures assumed in previous studies approximate folding of the lithosphere. Finally, using the intraplate deformation zone in the central Indian Ocean as an example, we address the conditions under which observed surface topography and surface strain can provide insight into the subsurface structure of large-scale folds.

Formulation

Finite Element Solutions for Finite Amplitude Folding

To calculate the deformation pattern in a horizontally shortening medium with an arbitrary, continuous viscosity stratification, we employ a finite element approach based on a penalty function formulation for viscous, incompressible flow. In this approach, the pressure term from the equilibrium equations is eliminated using the expression

$$u_{i,j} = -p/\chi \tag{1}$$

where χ is the penalty parameter that corresponds to a bulk viscosity of the material and u_i are the velocities. For large values of χ, the incompressibility condition $u_{i,i} = 0$ in the finite element solution is approximately satisfied [*e.g., Bathe*, 1982].

The effect of non-Newtonian rheology was included by implementing a simple incremental procedure [e.g., *Desai and Abel*, 1972] to calculate the viscosity at each time step or deformation increment. The model assumed a strain rate-dependent viscosity of the form

$$\mu = \mu_o \left[\frac{1}{\dot{\varepsilon}_2}\right]^{1-\frac{1}{n}} \tag{2}$$

where μ_o is the reference (initial) viscosity, ε_2 is the second invariant of the strain rate tensor, and n is the power law exponent of stress in the stress-strain rate relationship. To simulate the rheology of the lithosphere in the ductile creep regime, we used a power law exponent of ~3, while in the brittle regime we invoked the assumption of perfect plasticity in which $n \to \infty$ to approximate a material that deforms by pervasive faulting.

We used two approaches to calculate non-Newtonian deformation. In the first the viscosity was determined by stepping forward one-half time step, reforming the global stiffness matrix, calculating the viscosity field at the half time step and solving for the velocity field, then using the velocities at the half time step to advance the positions of the node points over the full time step. In the second approach we stepped forward one full time step and used the average strain rates from the current and previous time steps in reforming the global stiffness matrix and recalculating the velocity field. Then the solution for the velocity field was iterated until a convergence criterion was satisfied. In both approaches, the perturbed (non-Newtonian) viscosities were used at the next time step. We investigated models for various mesh resolutions, progressively increasing the number of elements in the mesh until the solutions no longer changed.

Boundary Conditions

The grid geometry and boundary conditions for the finite element model are shown schematically in Figure 2. The left boundary represents a symmetry plane on which the horizontal velocity u and shear stress τ vanish. The top boundary is stress free, and on the bottom boundary, τ and the vertical

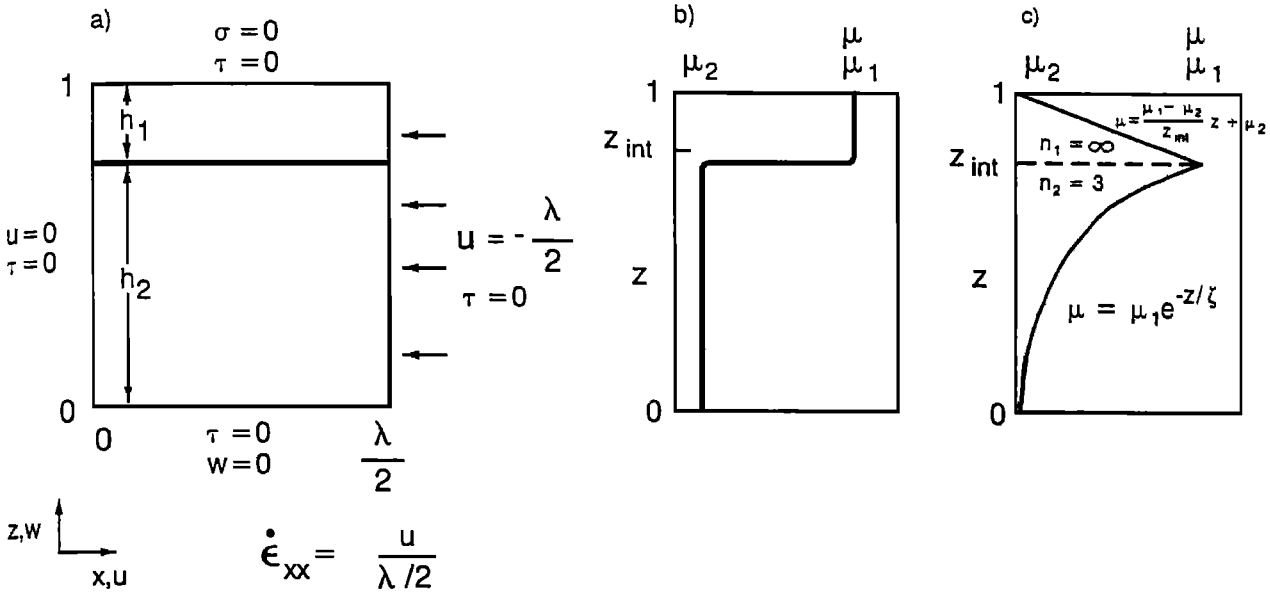

Figure 2. (a) Schematic of the finite element problem illustrating boundary conditions and normalization of the mean horizontal strain rate ε_{xx}. (b) Viscosity structure described by equation (6). (c) Viscosity structure for a strength envelope distribution of viscosity described by equation (7).

velocity w vanish. On the right boundary, τ vanishes and u is assigned a constant value. The horizontal and vertical grid dimensions were chosen to be $\lambda/2$ and 1, respectively. The dimension λ corresponded to the wavelength of the initial perturbation introduced. The values of the imposed horizontal velocity u were selected to yield a normalized horizontal strain rate ε_{xx} with a value of -1. This normalization permits growth rates determined from the finite element analysis to be directly compared to those from previous infinitesimal amplitude solutions [e.g., *Fletcher*, 1974, 1977; *Zuber*, 1986]. In the finite element models the growth rate q was determined from the slope of the relationship between the natural log of the root-mean-square (rms) amplitude of deformation and the mean horizontal strain $\varepsilon_{xx}t$ (see equation (4)).

Linearized Finite Amplitude Solutions

Determination of the dominant wavelength in a horizontally shortening, rheologically stratified medium entails solving the Navier-Stokes equations for plane, quasi-static flow. Analytical or nearly analytical solutions of these equations that are valid to first order in the perturbing flow have been obtained for media consisting of a layer of uniform strength that overlies a layer or halfspace in which strength is either uniform or decreases exponentially with depth (Figure 1a and 1b). Such solutions describe the initial stages of deformation, when the length scale of folding is presumably established [*Biot*, 1961]. The dominant wavelength, which is controlled by the thicknesses of the strong layers and other mechanical properties of the medium, corresponds to the wave number k_d or wavelength $\lambda_d = 2\pi/k_d$ at which the dimensionless growth rate q of the folding instability is maximized. For uniform horizontal compression, the growth rate is related to the amplitude of vertical displacement of a random initial perturbation, $\Delta_i(k,t)$, at the ith interface at time t by the expression

$$\Delta_i = \Delta_i(k,o)\exp\left[(1+q)\dot{\varepsilon}_{xx}t - 1\right] \tag{3}$$

where $\Delta_i(k,0)$ is the amplitude of the initial perturbation and $\dot{\varepsilon}_{xx}$ is the mean horizontal strain rate. Folding with a dominant wavelength develops when the magnitude of the initial perturbation amplifies with time, which occurs when the argument of the exponential term in (3) is greater than unity. The growth rate can be expressed by rearranging (3) to give

$$q = \frac{\ln\left[\Delta/\Delta_o\right]}{\dot{\varepsilon}_{xx}} - 1 \tag{4}$$

This parameter, which is nondimensionalized by ε_{xx}, provides a quantitative measure of the degree to which a medium is unstable with respect to folding, with fold development dynamically possible for $q>1$. The dominant wavelength λ_d corresponds to the wavelength at which q attains a maximum value for a given set of parameters that describe the thickness and viscosity structure of the medium.

Determination of the Dominant Wavelength

From linearized, infinitesimal amplitude solutions for simple lithosphere structures like Figures 1a and 1b, λ_d can be calculated directly by analytical methods. However, the wavelength of folding in more complex rheological models like Figure 1c must be determined numerically. Because in finite element models, grid dimensions often influence the wavelength that develops, we imposed the wavelength as an initial condition. In finite element models with viscosity distributions for which analytical solutions are available, the dominant wavelength from the analytical solution was imposed and the growth rate was calculated. The growth rates from the analytical and finite element solutions were then compared. For more complex viscosity structures, it was necessary to make an initial estimate of λ_d, calculate the growth rate, then vary λ_d until the value that amplified fastest was found. We imposed the initial wavelength in two ways. First, as illustrated in Figure 2, we defined the horizontal dimension of the grid to correspond to a half wavelength of deformation. Second, we defined an initial layer thickness perturbation d with a harmonic form

$$\delta = z_o + \Delta_o \cos\left[\frac{\pi x}{\lambda/2}\right]\sin\left[\frac{\pi z}{2}\right] \tag{5}$$

where z_0 represents the interface depth at which the perturbation was imposed, λ is the wavelength, and Δ_0 is a small (<<layer thickness) initial perturbation amplitude.

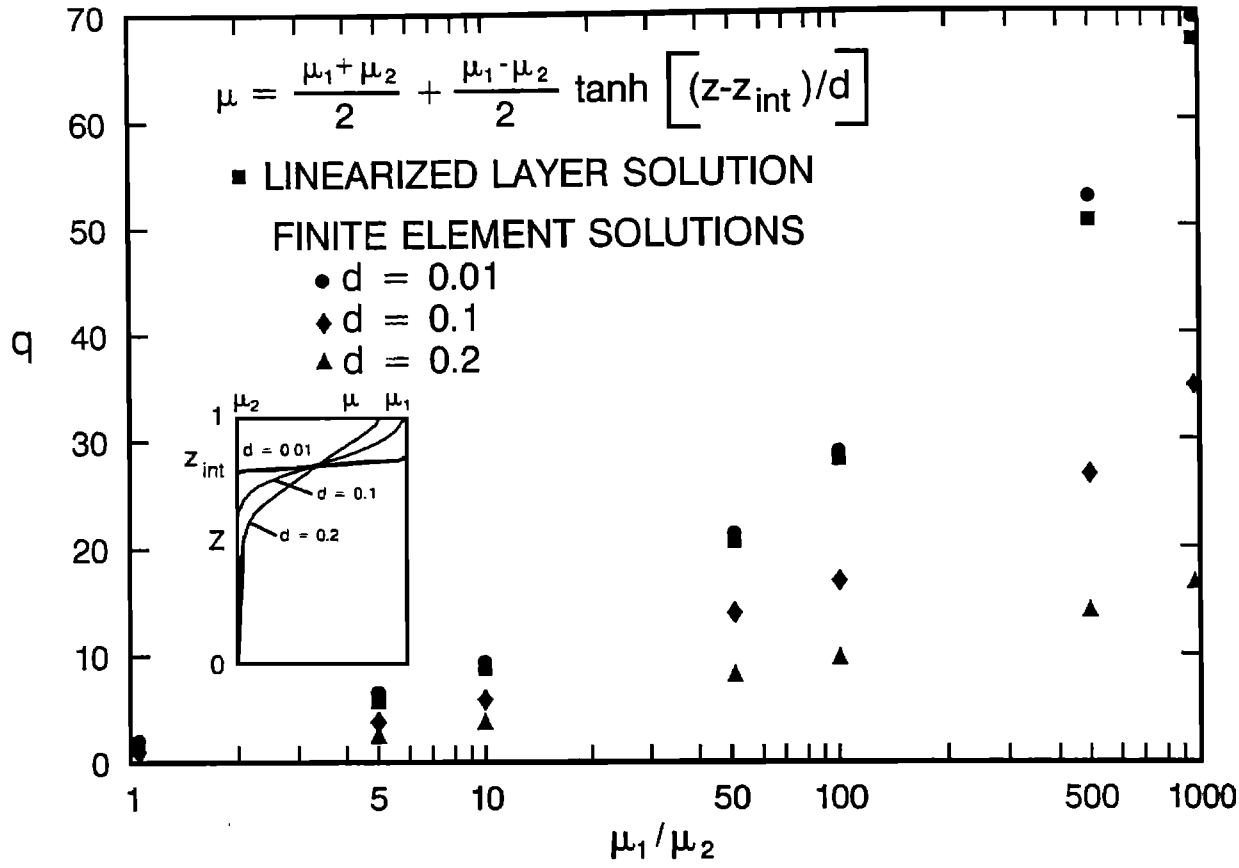

Figure 3. Comparison of linearized infinitesimal amplitude solution for high viscosity/low viscosity layer case and finite element solutions for the viscosity structures shown in the inset. For small d the viscosity structure in the finite element model approximates that of a high, uniform viscosity layer that overlies a low, uniform viscosity layer. For large d, the viscosity distribution displays a gradual gradation from high viscosity at the top to low viscosity at the bottom of the medium. The linearized solution agrees with the finite element solution in the limit of small d (~0.01). Note that for the range of cases examined the growth rates q exceed 1, indicating that the lithosphere is unstable with respect to folding. Parameters assumed in both the linearized and finite element solutions are μ_1/μ_2=100, z_{int}=0.8, and n_1=n_2=1.

Results

Uniform Viscosity Layer Models

In horizontally shortening media consisting of vertically stacked uniform viscosity layers, the growth of folding instabilities primarily reflects viscosity contrasts at layer interfaces. We wish to quantitatively assess the extent to which the driving force associated with a vertical discontinuity in viscosity within a layered medium is required for fold growth. To address this question, we investigated simple folding models for a Newtonian viscous lithosphere that consists of a high viscosity layer over a lower viscosity layer (Figure 1a). First, in order to test the accuracy of the finite element model, we compared growth rates calculated for a linearized infinitesimal amplitude analytical solution for this rheological structure to those determined for a numerical model with the same structure. We then analyzed the importance of viscosity discontinuities in driving fold growth by comparing these results to finite element solutions for structures with continuous viscosity variations.

To investigate the stability of both continuously and discontinuously stratified media, we assumed in the finite element models a viscosity distribution of the form (Figure 2b)

$$\mu = \frac{\mu_1+\mu_2}{2} + \frac{\mu_1-\mu_2}{2} \tanh\left[\frac{z-z_{int}}{d}\right] \quad (6)$$

where μ_1 and μ_2 are the viscosities at the top and bottom of the medium, z_{int} is the viscosity transition depth, and d defines the sharpness of the transition. The inset of Figure 3 shows plots of (6) for a range of d values. For small d the viscosity distribution corresponds to that for a medium with two layers of uniform viscosity with a viscosity contrast at the interface between the layers of μ_1/μ_2. Linearized solutions exist for this structure [*Fletcher*, 1977]. Larger d corresponds to a medium in which viscosity varies gradually with depth.

The net driving force for folding in a region of continous viscosity variation is the same as that across a discontinuity with the same net viscosity contrast. So long as the depth over which the viscosity varies is small compared to the wavelength of folding or the depth beneath the free surface of the viscosity variation, continuous and discontinuous viscosity variations should give essentially identical fold growth rates. Figure 3 shows results for three values of d along with the analytical infinitesimal amplitude solution for folding of a medium consisting of a strong uniformly viscous layer over a weak uniformly viscous layer (d=0). The finite

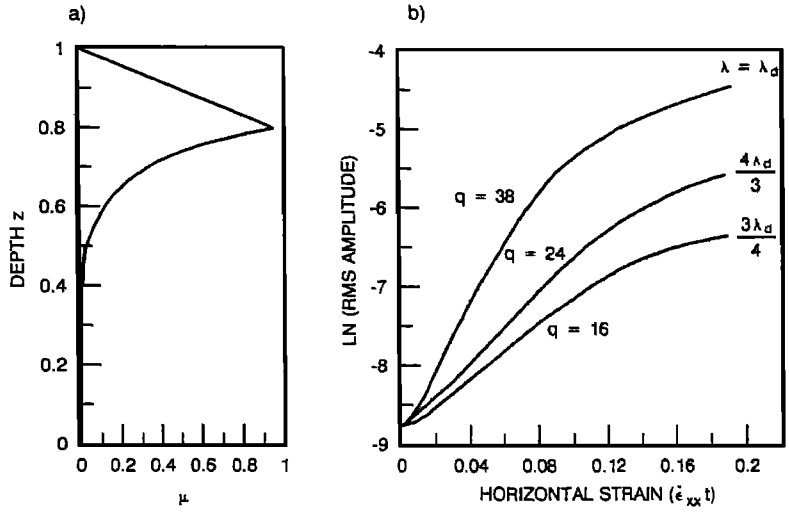

Figure 4. Determination of the dominant wavelength from growth rate curves. (a) Strength envelope viscosity distribution. (b) Relationships between rms amplitude and mean horizontal strain ($\dot{\epsilon}_{xx}t$) for model in Figure 4a. Solutions are shown for for three different imposed wavelengths λ. The dominant wavelength, λ_d/h_1=3.8, corresponds to the maximum growth rate of folding q, which is obtained from the slopes of the lines. Note that longer and shorter wavelengths yield smaller growth rates. Parameters in the solution include μ_1=100, μ_2=0, z_{int}=0.8, n_1=100, n_2=3, and z=0.1.

element solutions in the limit of small d can be compared to linearized solutions for layers bounded by discontinuities. Note that the analytical and finite element solutions for d=0.01 are in good agreement corresponding to a sharp falloff in viscosity with depth. The difference between the solutions at large μ_1/μ_2 and small d is a consequence of numerical resolution.

Figure 3 shows that previous linearized analytical solutions provide a reasonable approximation for the growth rate of folding for small strains. The amount of strain up to which the solutions agree is sensitive to details of the rheological structure, but the analytical and numerical growth rates generally agree to within approximately 15% up to strains of ~0.05 or more.

Growth rates for d=0.1 and 0.2 in Figure 3 are reduced because the depth scale of the viscosity is comparable to the layer thickness. However, even for the largest value of d shown (=0.2), which represents a very smoothly varying viscosity distribution, q exceeds unity for all μ_1/μ_2, which indicates that folding instabilities will amplify in the medium. Figure 3 quantitatively illustrates that sharp changes in viscosity favor the amplification of folding instabilities but that a discontinuity in viscosity is not required for folding. *Biot* [1960] came to a similar conclusion for the specific case of a compressing, continuously stratified viscoelastic half space in which viscosity decreased exponentially with depth. The present study shows that this conclusion holds for more general viscosity distributions.

Our approach for computing finite amplitude deformation differs from those used in previous models of folding of single layers. Finite amplitude folding has been examined via analytical theory for a uniform strength layer [*Chapple*, 1968] but did not treat general strength distributions. Past numerical studies [*Dieterich*, 1969; *Dieterich and Carter*, 1969; *Hudleston and Stephansson*, 1973; *Parrish*, 1973] did not make use of reduced integration on the penalty terms in the finite element formulation that allows accurate numerical calculation of the viscous flow field. In the limit of infinitesimal amplitude deformation, none of these studies accurately reproduced linearized analytical solutions [*Fletcher*, 1974].

Strength Envelope Models

The vertical distribution of strength in the lithosphere as constrained by laboratory experiments [*Byerlee*, 1968; *Brace and Kohlstedt*, 1980; *Kirby and Kronenberg*, 1987] is more complex than the viscosity structures assumed in previous lithospheric folding models, including those discussed above. Experiments indicate that strength in the shallow lithosphere in compression increases approximately linearly with depth due to the pressure dependence of brittle deformation and changes to a region in which strength decreases exponentially with depth due to the temperature dependence of ductile flow. A schematic of a simplified "yield strength envelope" for the lithosphere is shown in Figure 1c. The next objective of our study is to use the finite element approach to investigate deformation in a model lithosphere that incorporates this arguably more realistic strength envelope distribution of viscosity. In these models we incorporate nonlinear aspects of viscous flow, since $n \to \infty$ in the brittle regime and n~3 in the ductile flow regime.

Figs. 2a and 2c illustrate the boundary conditions, grid geometry, and physical parameters for the strength envelope model. For this structure the viscosity μ takes the form

$$\mu(z) = (\mu_1 - \mu_2)\frac{1-z}{1-z_{int}} + \mu_2 \qquad z \geq z_i \tag{7a}$$

in the brittle regime and

$$\mu(z) = \mu_1 \exp\frac{z - z_{int}}{\zeta} \qquad z \geq z_{int} \tag{7b}$$

in the ductile regime, where μ_1 is the viscosity at the brittle-ductile transition and μ_2 is the viscosity at the surface. The parameter z is the depth over which viscosity in the ductile regime falls by a factor of $1/e$, which approximates the temperature-dependence of viscosity .

The boundary conditions and grid geometry, shown in Figure 2, are the same as for the simpler Newtonian layer models discussed in the previous section. However, for the more complex rheological structures investigated in this section it was not possible to define the dominant wavelength a priori, using results from linearized infinitesimal amplitude solutions. Instead, it was necessary to make an initial guess as to the dominant wavelength, calculate q, and then change both the horizontal grid length and velocity of shortening in order to identify wavelengths that may have greater q values. Figure

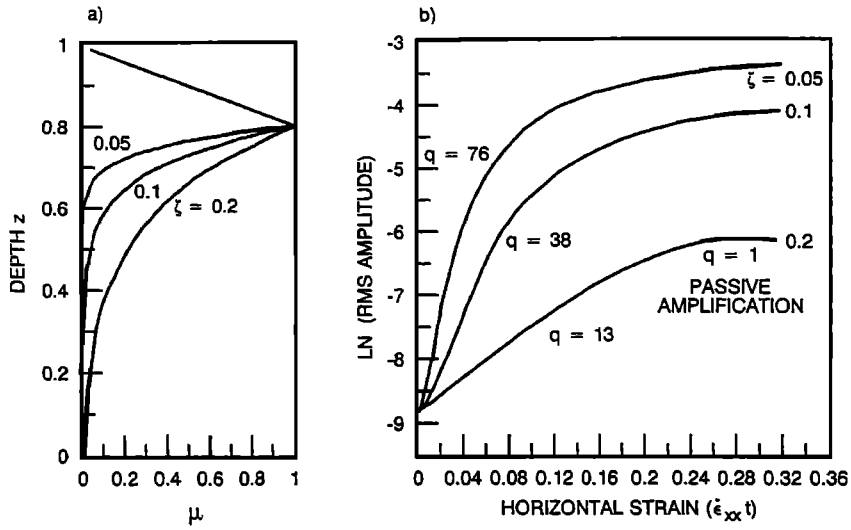

Figure 5. Figure 5b shows relationships between rms amplitude and mean horizontal strain $(\dot{\varepsilon}_{xx}t)$ for a shortening lithosphere with the viscosity structures in Figure 5a. The growth rates of folding q in Figure 5b are obtained from the slopes of the lines at strains <0.1. For all values of d, the slopes of the lines decrease at larger strains, indicating that q also decreases. For d=0.2, q decreases to the limiting value of 1, indicating that the medium no longer deforms by folding but solely by uniform horizontal shortening. Parameter values for this calculation are μ_1=100, μ_2=0, z_{int}=0.8, n_1=100, and n_2=3.

4b shows relationships between rms amplitude and mean horizontal strain $\varepsilon_{xx}t$ for a shortening lithosphere with the viscosity structure in Figure 4a. The initial growth rates of folding q are obtained from the slopes of the lines at strains <0.1. The solutions are for models assuming three different imposed wavelengths λ. The plot shows that different growth rates are obtained for different wavelengths of folding. The wavelength corresponding to the maximum value of q is the dominant wavelength. Wavelengths that are longer ($\lambda=4\lambda_d/3$) or shorter ($\lambda=3\lambda_d/4$) than the dominant wavelength have shallower slopes and correspondingly smaller growth rates.

Figure 5 shows estimates of q for folding at the dominant wavelength for three viscosity distributions with fixed thickness and viscosity structure in the brittle layer and different values of z of the ductile layer. In each case, q exceeds the critical value of one, which indicates that lithospheres with all of these viscosity distributions fold (rather than shorten uniformly) when horizontally shortened. As for the infinitesimal amplitude solutions [*Biot*, 1960; *Zuber*, 1987b], the rate of fold growth is greater for smaller z. The solutions in Figures 4 and 5 demonstrate that a medium with a viscosity distribution that approximates the vertical distribution of strength in the lithosphere can develop folds when horizontally shortened.

Both Figures 4 and 5 illustrate that with decreasing z, q progressively decreases with increasing horizontal strain $\varepsilon_{xx}t$, which indicates that folds will grow more slowly with increasing strain. In fact, for the case of z=0.2, q decreases to the limiting value of 1. This corresponds to purely passive amplification in which the folds grow at a rate equal to the rate of horizontal shortening. Deformation of the medium in that case is accommodated solely by uniform thickening of the medium rather than by a combination of thickening and folding.

Topography, Surface Strain, and Crustal Thickness

In outcrop-scale folding models, observations of the wavelength and thickness of the folded layer provide information on the viscosity contrast between the layer and its surrounding matrix [*Biot*, 1957; *Johnson*, 1970]. For folding on the scale of the lithosphere, however, only the wavelength is directly observed; details of the lithosphere strength structure are sought from the models. We are thus motivated to assess whether other observed aspects of the deformation can provide additional constraints on the subsurface structure.

Figure 6a shows the deformation pattern, as derived from the velocity field, associated with folding of a model lithosphere consisting of a strong, uniform viscosity layer that overlies a weaker viscous layer for a mean horizontal strain of 0.2. Deformation occurs by flexural folding in which the layer bends sinusoidally while retaining constant thickness. Figure 6b shows the effect of folding of a lithosphere with a strength envelope distribution of viscosity for the same mean strain. In this case the weak area near the surface concentrates strain as horizontal shortening progresses, particularly in fold troughs. Folds in the strength envelope model are thus characterized by layer thickening beneath topographic lows. While the deformation patterns in the two models are distinctive, it is not clear whether the models could be distinguished on the basis of their surface topographic expressions alone. The presence or absence of crustal thickening beneath topographic lows, however, which could be detected from seismic imaging of the crust, could be diagnostic of the rheological structure.

Distributions of surface strain associated with the model viscosity distributions for the same conditions as above are shown in Figure 7. The models show a similar dynamic range of surface strain, but the distribution of strain along the fold differs in the models. In the uniform viscosity layer model (Figure 7a) flexural bending of the layer results in a state of extension in the topographic highs and compression in topographic lows. In the strength envelope model (Figure 7b) the low strength near the surface relative to that deeper in the brittle layer results in a state of compression everywhere along the fold, with the greatest amount of shortening in topographic lows. In this model more strain at the surface is accommodated by penetrative shortening relative to layer bending than in the uniform viscosity model. However, as shown in Figure 6b, the amount of flexural bending in the strength envelope model increases significantly over that at

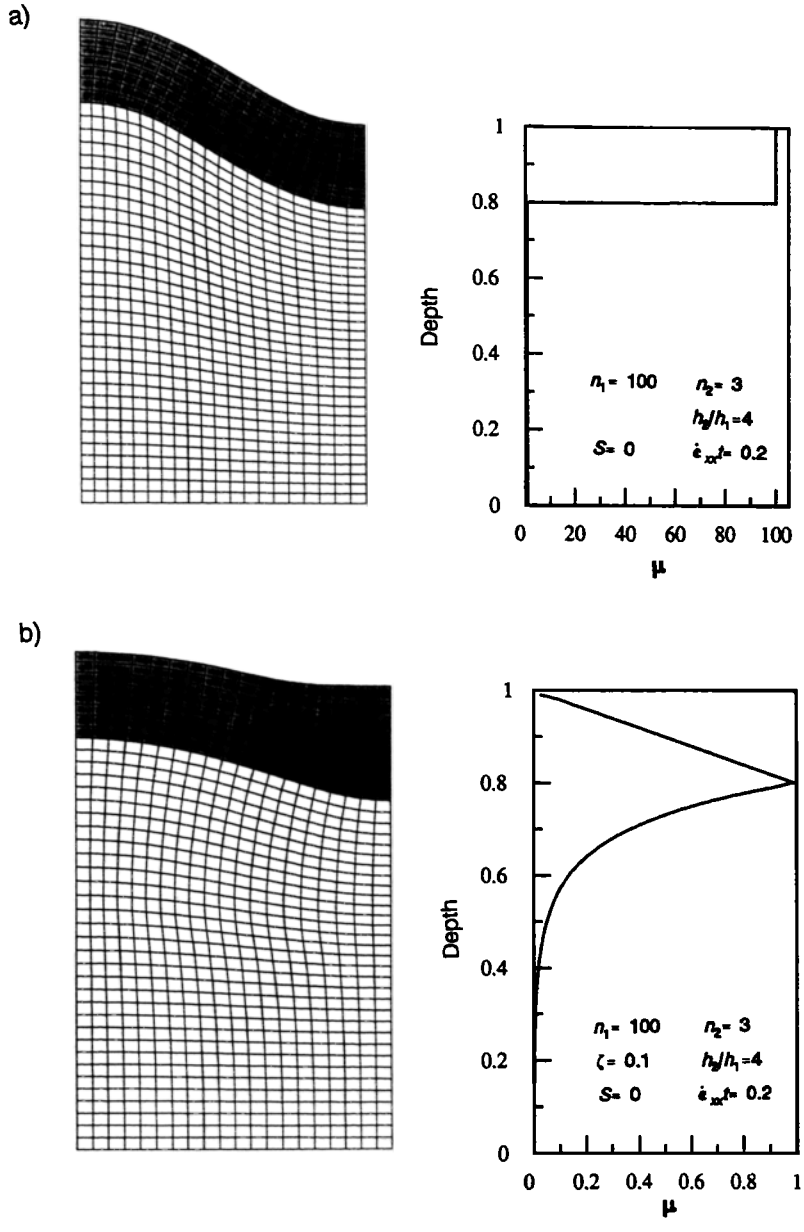

Figure 6. (a) Deformation of a model lithosphere consisting of a highly non-Newtonian (brittle) surface layer of uniform viscosity (shaded) that overlies a weaker non-Newtonian uniform viscosity layer. Deformation grid is on left and viscosity structure is on right. The surface layer deforms by flexural folding characterized by bending with no change in layer thickness. Parameter values assumed include μ_1/μ_2=100, z_{int}=0.8, n_1=100, n_2=3, S=0, and $\dot{\epsilon}_{xx}t = 0.2$. (b) Deformation of a model lithosphere with a strength envelope distribution of viscosity. In this case the brittle surface layer (shaded) deforms by folding characterized by layer thickening beneath topographic lows. Parameter values are μ_1=200, μ_2=1, z_{int}=0.8, n_1=100, n_2=3, z=0.1, S=0, and $\varepsilon_{xx}t = 0.2$.

the surface in the strong brittle/ductile core of the lithosphere. These differences persist over a range of model parameters and suggest that observed distributions of surface strain may be diagnostic of the subsurface strength stratification.

Application to Folding in the Central Indian Ocean

Seafloor folding in the central Indian Ocean is a well-expressed and well-studied example of intraplate deformation of oceanic lithosphere [*Weissel et al.*, 1980]. Deformation in this area is characterized by east-west trending topographic undulations with a wavelength of 100-300 km and amplitudes of the order of 1-2 km [*Weissel et al.*, 1980; *Geller et al.*, 1983; *Neprochnov et al.*, 1988]. Large-amplitude, E-W trending gravity and geoid anomalies also characterize the deformation [*Weissel and Haxby*, 1984; *McAdoo and Sandwell*, 1985]. Understanding of the nature of horizontal shortening in this region would constrain the kinematics of Indo-Australian plate deformation [e.g., *Wiens et al.*, 1985; *Stein et al.*, 1990; *Royer and Chang*, 1991] as well as the

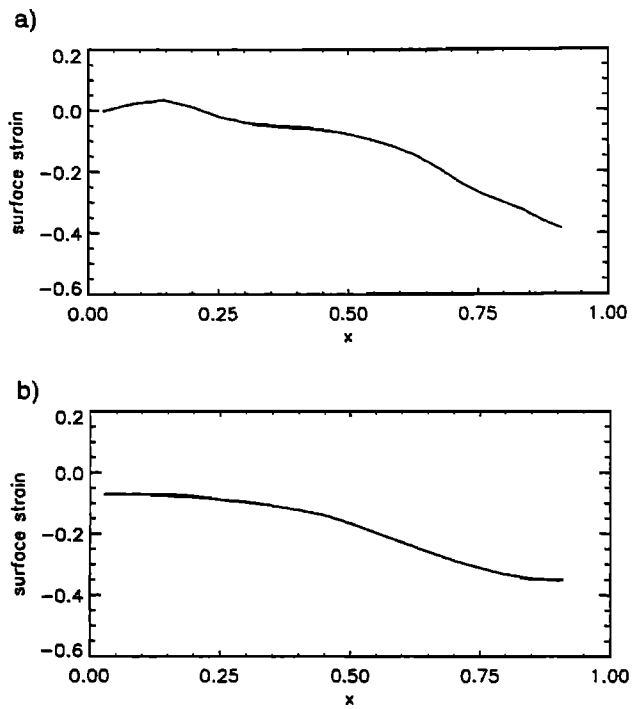

Figure 7. Distribution of surface strain associated with deformation in Figure 6.

rheology of the lithosphere [*McAdoo and Sandwell*, 1985; *Zuber*, 1987b; *Karner and Weissel*, 1990a].

A finite amplitude flexure model has previously been applied to the Indian Ocean deformation [*Karner and Weissel*, 1990a] which addressed why the deformation localized where it did. This model also constrained the force per unit length associated with the deformation. However, that model contained thin plate approximations and did not address details of the rheological structure and their relationship to the deformation. One of the principal outcomes of the analysis presented in this paper is the prediction, for a lithosphere characterized by a strength envelope distribution of viscosity, of thickening of the plastic layer beneath fold trough (Figure 6c). This is in contrast to previous uniform viscosity layer formulations [*Zuber*, 1987b; *Martinrod and Davy*, 1992] which predict either (constant layer thickness) buckling for a strong surface layer or layer thickening beneath the ridge for a weak surface layer. *Louden* [1995] has calculated crustal structure through analysis of seismic refraction and gravity data for a typical ridge-trough feature in the Indian Ocean deformation zone and has reported the crust to be 0.5-1 km thinner beneath the ridge as compared to the trough. He ascribed the variation in structure to either lateral flow of serpentinite in the lower crust, or possibly asymmetric folding due to an unspecified mechanism. We contend that such a mode of deformation is a natural consequence of horizontal shortening of a lithosphere with a strength envelope viscosity structure. A more detailed seismic and gravity survey would provide the basis for testing whether such structure is observed in other areas of the deformation zone.

Another key question is the nature of strain accommodation. Strain estimates for the region have varied considerably, with values <1% derived from seismic moment tensors [*Stein and Okal*, 1978; *Petroy and Wiens*, 1989] and values up to 10% from plate kinematic models [*Wiens et al.*, 1985; *DeMets et al.*, 1988, 1990; *Gordon et al.*, 1990]. More recently, horizontal strains have been estimated to be of order 2-5% from single- and multi-channel seismic profiles [*Bull and Scrutton*, 1990, 1992; *Chamot-Rooke et al.*, 1993; *Van Orman et al.*, 1995].

Analyses based on single channel seismic reflection data from the deformation zone [*Weissel et al.*, 1981; *Geller et al.*,

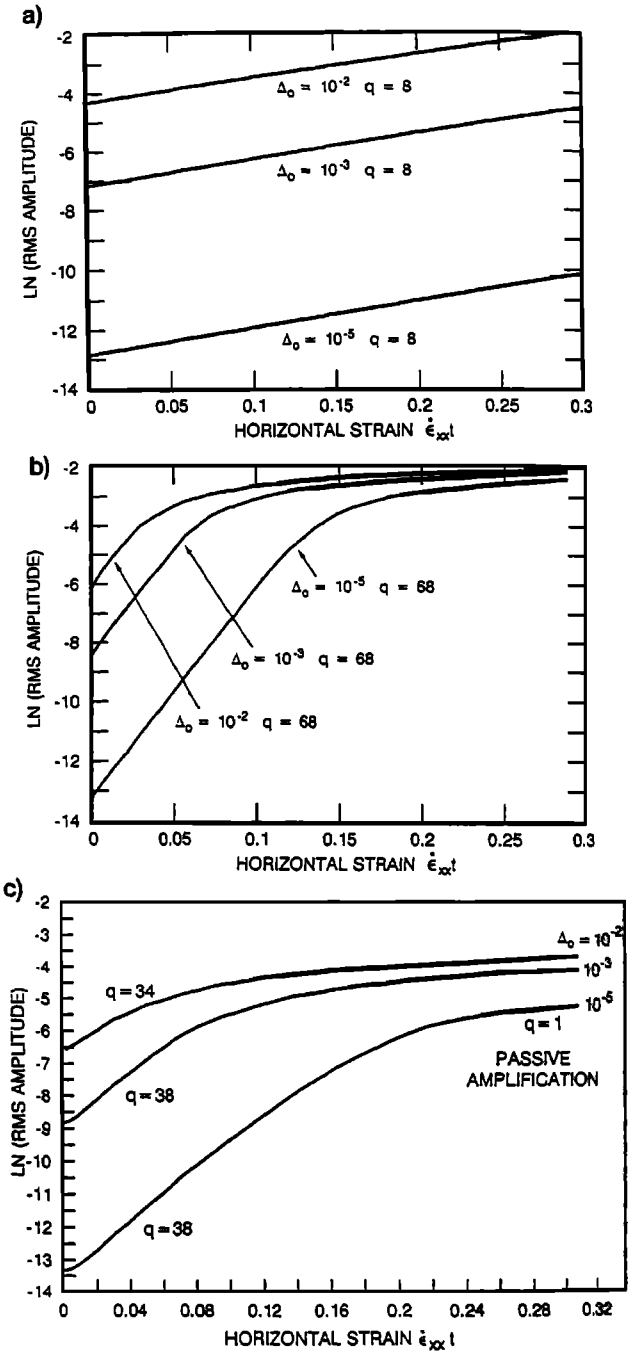

Figure 8. Relationships between rms amplitude and mean horizontal strain $(\dot{\epsilon}_{xx}t)$ for three values of the initial perturbation amplitude (Δ_0) for three model lithospheres with continuous viscosity distributions. (a) Solutions are for Newtonian viscous lithosphere with μ_1=10, μ_2=1, z_{int}=0.8, z=0.01. Note that the lines have different y axis intercepts but the same slopes for all $\varepsilon_{xx}t$. indicating that the growth rate of the instability q is independent of the amplitude of the initial perturbation for the full range of strain examined. However, the relationship between rms amplitude and horizontal strain is dependent on Δ_0 over the range of strains. (b) Same as Figure 8a except μ_1=1000, μ_2=1, z_{int}=0.8, and z=0.01. For horizontal strains >0.1, a given amplitude implies a particular strain, independent of Δ_0. (c) Non-Newtonian lithosphere with a strength envelope distribution of viscosity assuming μ_1=1, μ_2=0, z_{int}=0.8, z=0.1, n_1=100, and n_2=3. Here q is independent of Δ_0 at small strains, but the relationship between rms amplitude and horizontal strain is dependent on Δ_0 over the range of strains.

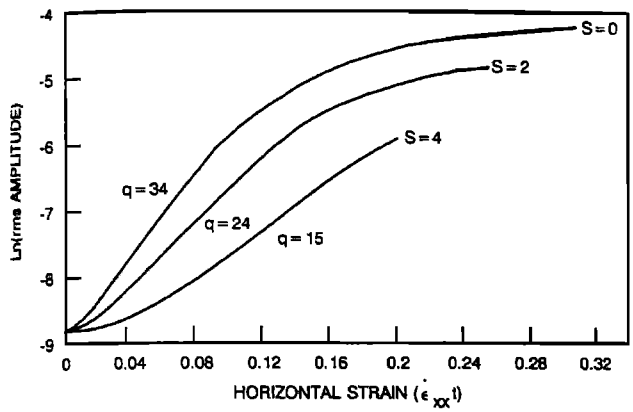

Figure 9. Relationships between rms amplitude and mean horizontal strain $(\dot{\bar{\varepsilon}}_{xx}t)$ for three values of the buoyancy/strength parameter S $(=\rho_1 g h_1/2\mu\dot{\varepsilon}_{xx})$ where ρ_1 and h_1 are the density and thickness of the surface layer. Calculation assumes μ_1=1, μ_2=0, z_{int}=0.8, z=0.1, n_1=100, and n_2=3. Note that even for large S, q>1, which indicates that the medium is unstable with respect to folding.

1983; *Chamot-Rooke et al.*, 1993] found strain due to faulting to be of order 10^{-2} and that due to folding to be 10^{-3} or less. Strain accommodation by faulting was estimated from observed fault offsets, but strain accommodation via continuum shortening is more challenging to constrain. Systematically mapping crustal thickness variations in the region would be a particularly desirable approach to acquiring more confident estimates. Models like those considered in this study could relate the amplitude of surface topography to the horizontal strain for a given rheological structure and thus may contribute to the understanding of strain accommodation in the Indian Ocean deformation zone. If one uses as a constraint published estimates of total strain in this region, then our models can provide insight into lithosphere rheology if the amplitude of folding is independent of the amplitude of the initial perturbation. The approach assumes that slip along faults occurs along plastic slip lines in brittle regions which are at yield and thus pervasively deforming, so it is possible to investigate regional averages but not strain associated with individual faults.

Figure 8 shows calculated fold amplitudes as a function of horizontal strain for three different viscosity models, each with a range of initial perturbation amplitudes Δ_o. Figs. 8a and 8b are for a lithosphere with uniform viscosity Newtonian layers such as shown in Figure 2b with μ_1/μ_2=10 and 1000, respectively. Figure 8c is for a lithosphere with a strength envelope distribution of viscosity as shown in Figure 2c. For μ_1/μ_2=10, the ampitude is a strong function of the initial perturbation, with higher topographic amplitudes for larger initial perturbation amplitudes over the range of strain. For the higher viscosity contrast in Figure 8b, the solution shows the same behavior at low horizontal strains (0.1). However, at larger strains topographic amplitude becomes independent of the amplitude of the initial perturbation. For these cases, in the absence of erosion it would be possible to estimate the horizontal strain associated with folding from the bathymetric amplitudes of the folds. As shown in Figure 8c, the topographic amplitude for a strength envelope distribution of viscosity becomes less sensitive to the initial perturbation amplitude at high strains, but it never becomes independent of it. In this case, there is no unique relationship between fold amplitude and horizontal shortening that is independent of the physical factors present as folding initiated. For the typical amplitude of seafloor topography for oceanic lithosphere created at the appropriate spreading rate, the average seafloor roughness at the wavelength of Indian Ocean folding is in the range 50-100 m [*Goff*, 1991; *Hayes and Kane*, 1991; *Maliverno*, 1991]. If Indian Ocean seafloor, before folding, was typical, estimates of horizontal strain could be derived for the complete range of models described in this study. For example, for a model lithosphere with a rheological structure of seafloor with an age corresponding to that in the Indian Ocean at the onset of folding, a horizontal strain of ~6% is implied for $\Delta_o/\Delta=10^{-2}$, which is in agreement with the seismic reflection estimates. With knowlege of the crustal thickness, regional studies relating strain to rheological structure would be possible.

Buoyancy forces, which would act to resist fold growth, have been neglected in the above models. The effect of buoyancy can be quantitatively evaluated by varying the dimensionless parameter, $S=\rho_1 g h_1/2\mu\dot{\varepsilon}_{xx}$, where ρ_1 and h_1 are the density and thickness of the surface layer, represents the ratio of the buoyancy force due to layer thickness variations normalized by the average strength of the surface layer. Small S (~0) corresponds to the limit of a strong layer in which buoyancy forces are small in magnitude and do not influence the perturbing velocity field. Large S corresponds to the limit of a weak layer in which buoyancy forces significantly affect the pattern of flow. Figure 9 shows solutions for three S values and illustrates the effect of buoyancy in damping folding instabilities. As buoyancy forces become increasingly important (larger S), q progressively decreases, indicating that folds with smaller topographic amplitudes will develop. However, for the structures we investigated, buoyancy forces are not large enough in magnitude in comparison to lithospheric strength to prevent folding. For values of S on the order of unity, required to explain the wavelength of lithospheric folding in the Indian Ocean [*Zuber*, 1987b], gravity only slightly reduces the growth rate.

Conclusions

To better understand the mechanics of finite amplitude lithospheric-scale folding, we used finite element solutions to study the development of folds in model lithospheres characterized by both discontinuous and continuous viscosity distributions and with strongly strain rate-dependent rheologies that approximate slip on prevasively destributed faults. First, we examined the folding of a Newtonian viscous medium that contains discontinuities in viscosity and compared the results to existing linearized, infinitesimal amplitude solutions. Growth rates predicted by the finite element solutions for horizontal strains up to 0.05 or more agree to within approximately 15% with those predicted from infinitesimal amplitude solutions. Our results thus demonstrate that previous linearized models of folding provide a reasonable approximation of the physics of the growth of folds for small strains.

In both infinitesimal amplitude and finite element models of folding with layers of uniform, contrasting viscosities, folding is driven solely by the magnitudes of discontinuities in viscosity at layer interfaces. However, our finite element solutions show that media with continuous viscosity distributions, including structures that approximate the distribution of strength in the lithosphere as indicated by laboratory experiments, can also be unstable with respect to folding. The net driving force for folding in a region of continous viscosity variation is the same as the driving force across a discontinuity with the same net viscosity contrast. Continuous and discontinuous viscosity variations give essentially identical fold growth rates if the depth over which the viscosity varies is small compared to the wavelength of folding or the depth beneath the surface of the viscosity variation. While a uniform viscosity layer in horizontal compression will deform flexurally (*i.e.*, no change of layer thickness) for a strong layer and by inverse boudinage (*i.e.*, layer thicknening under topographic highs) for a weak layer, a lithosphere with a strength envelope distribution of lithosphere viscosity exhibits excess thickening of the layer beneath the topographic low. This structure has been observed in the intraplate deformation zone in the central Indian Ocean.

For both Newtonian and non-Newtonian models with continuous viscosity distributions, growth rates of folding are

independent of initial conditions for small strains. However, the relationship between topographic amplitude and horizontal strain is sensitive to initial conditions, except for models with high viscosity contrasts (μ_1/μ_2~1000) at high strains (0.1). Thus, estimates of horizontal strain from the topographic expression of folding alone may be possible if the dynamic range of initial surface topography with length scales comparable the dominant wavelength can be reasonably bounded. Buoyancy forces slow the rate of fold amplification, but are inadequate to prevent folding for a range of realistic lithospheric structures.

Acknowledgments. This work was supported by a NASA Geodynamics Program grant to M.T.Z. and a NASA Planetary Geology and Geophysics Program Grant to E.M.P. We are grateful for helpful reviews from J. Weissel, L. Dell'Angelo, and an anonymous reviewer. M.T.Z. acknowledges helpful discussions with Seth and Carol Stein during their sabbatical at the Goddard Space Flight Center.

References

Bathe, K.-J., *Finite Element Procedures in Engineering Analysis*, 735 pp., Prentice-Hall, Englewood Cliffs, N.J., 1982.

Biot, M.A., Instability of a continuously inhomogeneous viscoelastic half-space under initial stress, *J. Franklin Inst., 270*, 190-201, 1960.

Biot, M.A., Folding instability of a layered viscoelastic medium under compression, *Proc. R. Soc. London A, 242*, 444-454, 1957.

Biot, M.A., Theory of folding of stratified viscoelastic media and its implications in tectonics and orogenesis, *Geol. Soc. Am. Bull., 72*, 1595-1620, 1961.

Brace, W.F., and D.L. Kohlstedt, Limits on lithospheric stress imposed by laboratory experiments, *J. Geophys. Res., 85*, 6248-6252, 1980.

Bull, J.M., and R.A. Scrutton, Fault reactivation in the central Indian Ocean and the rheology of oceanic lithosphere, *Nature, 344*, 855-858, 1990.

Bull, J.M., and R.A. Scrutton, Seismic reflection images of intraplate deformation, central Indian Ocean, and their tectonic significance, *J. Geol. Soc. London, 149*, 955-966, 1992.

Byerlee, J.D., Brittle-ductile transition in rocks, *J. Geophys. Res., 73*, 4741-4750, 1968.

Campbell, D.B., J.W. Head, J.K., Harmon, and A.A. Hine, A.A., Venus: Indentification of banded terrain in the mountains of Ishtar Terra, *Science, 221*, 644-647, 1983.

Chamot-Rooke, N., F. Jestin, B. de Voogd, and Phedre Working Group, Intraplate shortening in the central Indian Ocean determined from a 2100-km-long north-south deep seismic reflection profile, *Geology, 21*, 1043-1046, 1993.

Chapple, W.M., A mathematical theory of finite-amplitude rock-folding, *Geol. Soc. Am. Bull., 79*, 47-68, 1968.

DeMets, C., R.G. Gordon, and D.F. Argus, Intraplate deformation and closure of the Australia-Antarctica-Africa plate circuit, *J. Geophys. Res., 93*, 11,877-11,897, 1988.

DeMets, C., R.G. Gordon, D.F. Argus, and S. Stein, Current plate motions, *Geophys. J. Int., 101*, 425-478, 1990.

Desai, C.S,. and J.F. Abel, *Introduction to the Finite Element Method*, 477 pp., Van Nostrand Reinhold, New York, 1972.

Dieterich, J.H., Origin of cleavage in folded rocks, *Am. J. Sci., 267*, 155-165, 1969.

Dieterich, J.H ., and N.L. Carter, Stress-history of folding, *Am. J. Sci., 267*, 129-154, 1969.

Fletcher, R.C., Wavelength selection in folding of a single layer with power-law rheology, *Am. J. Sci., 274*, 1029-1043, 1974.

Fletcher, R.C., Folding of a single, viscous layer: Exact infinitesimal-amplitude solution, *Tectonophysics*, 39, 593-606, 1977.

Geller, C.A., J.K. Weissel, and R.N. Anderson, Heat transfer and intraplate deformation in the central Indian Ocean, *J. Geophys. Res., 88*, 1018-1032, 1983.

Goff, J.A., A global and regional stochastic analysis of near-ridge abyssal hill morphology, *J. Geophys. Res., 96*, 21,713-21,737, 1991.

Gordon, R.G., C. DeMets, and D.F. Argus, Kinematic constraints on distributed lithospheric deformation in the equatorial Indian Ocean from present motion between the Australian and Indian plates, *Tectonics, 9*, 409-422, 1990.

Hayes, D.E., and K.A. Kane, The dependence of seafloor roughness on spreading rate, *Geophys. Res. Lett., 18*, 1425-1428, 1991.

Hudleston, P.J., and O. Stephansson, Layer shortening and fold-shape development in the buckling of single layers, *Tectonophysics, 17*, 299-321, 1973.

Johnson, A.M., *Physical Processes in Geology*, 576 pp., W.H. Freeman, New York, 1970.

Karner, G.D, and A.B. Watts, Gravity anomalies and flexure of the lithosphere at mountain ranges, *J. Geophys. Res., 88*, 10,449-10,447, 1983.

Karner, G.D., and J.K. Weissel, Factors controlling the location of compressional deformation of oceanic lithosphere in the central Indian Ocean, *J. Geophys. Res., 95*, 19,795-19,810, 1990a.

Karner, G.D., and J.K. Weissel, Compressional deformation of oceanic lithosphere in the central Indian Ocean: Why it is where it is, *Proc. Ocean Drill. Program Sci. Results, 116*, 279-289,1 990b.

Kirby, S.H., and A.K. Kronenberg, Rheology of the lithosphere: Selected topics, *Rev. Geophys., 25*, 1219-1244, 1987.

Lambeck, K., The role of compressive forces in intracratonic basin formation and mid-plate orogenies, *Geophys. Res. Lett., 10*, 845-848, 1983.

Louden, K.E., Variations in crustal structure related to intraplate deformation: Evidence from seismic refraction and gravity profiles in the central Indian Ocean, *Geophys. J. Int., 120*, 375-392, 1995.

Maliverno, A., Inverse square-root dependence of mid-ocean-ridge flank roughness on spreding rate, *Nature, 352*, 58-60, 1991.

Martinod, J., and P. Davy, Periodic instabilities during compression or extension of the lithosphere, 1, Deformation modes from an analytical perturbation method, *J. Geophys. Res., 97*, 1999-2014, 1992.

McAdoo, D.C., and D.T. Sandwell, Folding of oceanic lithosphere, *J. Geophys. Res., 90*, 8563-8568, 1985.

Neprochnov, Y.P., O.V. Levchenko, L.R. Merklin, and V.V. Sedov, The structure and tectonics of the intraplate deformation area in the Indian Ocean, *Tectonophysics, 156*, 89-106, 1988.

Neumann, G.A., and M.T. Zuber, A continuum approach to the development of normal faults, *Proc. U.S. Symp. Rock Mech, 35th*, 191-198, 1995.

Parrish, D.K., A nonlinear finite element fold model, *Am. J. Sci., 273*, 318-334, 1973.

Petroy, D.E., and D.A. Wiens, Historical seismicity and implications for diffuse plate convergence in the northeast Indian Ocean, *J. Geophys. Res., 94*, 12,301-12,319, 1989.

Platt, J.P., B. Van den Eeckhout, E. Janzen, G. Konert, O.J. Simon, and R. Weijermars, The structure and tectonic evolution of the Aguilon fold nappe, Sierra Alhamilla, Betic Cordilleras, S.E. Spain, *J. Struct. Geol., 5*, 519-538, 1983.

Ricard, Y., and C. Froidevaux, Stretching instabilities and lithospheric boudinage, *J. Geophys. Res., 91*, 8314-8324, 1986.

Royer, J.-Y., and T. Chang, Evidence for relative motions between the Indian and Australian plates during the last 20 Myr from plate tectonic reconstructions: Implications for deformation of the Indo-Australian plate, *J. Geophys. Res., 96*, 11,799-11,802, 1991.

Stein, C.A., S. Cloetingh, and R. Wortel, Kinematics and mechanics of the Indian Ocean diffuse plate boundary zone, *Proc. Ocean Drill. Program,Sci. Results, 116*, 261-277, e1990.

Stein, S., and E.A. Okal, Seismicity and tectonics of the Ninetyeast Ridge area: Evidence for internal deformation of the Indian plate, *J. Geophys. Res., 83*, 2233-2246, 1978.

Turcotte, D.L., and G. Schubert, *Geodynamics: A Continuum Approach to Geological Problems*, 450 pp., John Wiley, New York, 1982.

Van Orman, J., J.R. Cochran, J.K. Weissel, and F. Jestin, Distribution of shortening in the Indo-Australian plate, *Earth Planet. Sci. Lett.*, in press, 1995.

Weissel, J.K., R.N. Anderson, and C.A. Geller, Deformation of the Indo-Australian plate, *Nature, 287*, 284-291, 1980.

Weissel, J.K., R.N. Anderson, and C.A. Geller, Preliminary results of the 1980 shipboard investigation of deformation of the Indo-Australian plate, I, Seismic reflection, *Eos Trans. AGU, 62*, 404, 1981.

Weissel, J.K., and W.F. Haxby, A tectonic tour of the Indian Ocean via the Seasat satellite, *Eos Trans. AGU, 65*, 185, 1984.

Wiens, D.A., C. DeMets, R.G. Gordon, S. Stein, D. Argus, J.F. Engeln, P. Lundgren, D. Quible, C. Stein, S. Weinstein, and D.F. Woods, A diffuse plate boundary model for Indian Ocean tectonics, *Geophys. Res. Lett., 12*, 429-432, 1985.

Zuber, M.T., Unstable deformation in layered media: applications to planetary lithospheres, 126 pp., Ph.D. thesis, Brown Univ., Providence, R.I., 1986.

Zuber, M.T., Constraints on the lithospheric structure of Venus from mechanical models and tectonic surface features, *Proc. Lunar Planet. Sci. Conf. 17th, Part 2, J. Geophys. Res., 92, Suppl.*, E541-E551, 1987a.

Zuber, M.T., Compression of oceanic lithosphere: An analysis of intraplate deformation in the central Indian Basin, *J. Geophys. Res., 92*, 4817-4825, 1987b.

Zuber, M.T., and L.L. Aist, The shallow structure of the Martian lithosphere in the vicinity of the ridged plains, *J. Geophys. Res., 95*, 14,215-14,230, 1991.

E.M Parmentier, Department of Geological Sciences, Box 1846, Brown University, Providence, RI 02912.

M.T. Zuber, Department of Earth, Atmospheric, and Planetary Sciences, Massachusetts Institute of Technology, 54-518, Cambridge, MA 02139-4307. (e-mail: zuber@mit.edu)

(Received December 5, 1994; revised July 11, 1995;
accepted August 11, 1995.)